Chinese Journal of Natural Medicines

Palmitic acid reduces the methylation of the FOXO1 promoter to suppress the development of diffuse large B-cell lymphoma *via* modulating the miR-429/DNMT3A axis

Weiming LI, Ming GAO, Weili XUE, Xiaoli LI, Yu CHANG, Kaixin ZHANG, Chenyu WEN, Mingzhi ZHANG

Citation: Weiming LI, Ming GAO, Weili XUE, Xiaoli LI, Yu CHANG, Kaixin ZHANG, Chenyu WEN, Mingzhi ZHANG, Palmitic acid reduces the methylation of the FOXO1 promoter to suppress the development of diffuse large B-cell lymphoma *via* modulating the miR-429/DNMT3A axis, Chinese Journal of Natural Medicines, 2024, 22(6), 554-567. doi: 10.1016/S1875-5364(24)60655-2.

View online: https://doi.org/10.1016/S1875-5364(24)60655-2

Available online at www.sciencedirect.com
ScienceDirect
Chinese Journal of Natural Medicines 2024, **22**(6): 554-567
doi: 10.1016/S1875-5364(24)60655-2
Chinese Journal of Natural Medicines

•Original article•

Palmitic acid reduces the methylation of the FOXO1 promoter to suppress the development of diffuse large B-cell lymphoma *via* modulating the miR-429/DNMT3A axis

LI Weiming[1], GAO Ming[2], XUE Weili[2], LI Xiaoli[2], CHANG Yu[2], ZHANG Kaixin[1], WEN Chenyu[1], ZHANG Mingzhi[2*]

[1] *Department of Oncology, Henan University of Traditional Chinese Medicine, Zhengzhou 450000, China;*
[2] *Department of Oncology, The First Affiliated Hospital of Zhengzhou University, Zhengzhou 450000, China*

Available online 20 Jun., 2024

[ABSTRACT] Diffuse large B-cell lymphoma (DLBCL) is characterized by significant treatment resistance. Palmitic acid (PA) has shown promising antitumor properties. This study aims to elucidate the molecular mechanisms by which PA influences DLBCL progression. We quantified the expression levels of microRNAs (miRNAs), Forkhead box protein O1 (FOXO1), and DNA methyltransferase 3A (DNMT3A) in both untreated and PA-treated DLBCL tumors and cell lines. Assessments were made of cell viability, apoptosis, and autophagy-related protein expression following PA administration. Interaction analyses among miR-429, DNMT3A, and FOXO1 were conducted using luciferase reporter assays and methylation-specific (MSP) Polymerase chain reaction (PCR). After transfecting the miR-429 inhibitor, negative control (NC) inhibitor, shRNA against DNMT3A (sh-DNMT3A), shRNA negative control (sh-NC), overexpression vector for DNMT3A (oe-DNMT3A), or overexpression negative control (oe-NC), we evaluated the effects of miR-429 and DNMT3A on cell viability, mortality, and autophagy-related protein expression in PA-treated DLBCL cell lines. The efficacy of PA was also tested *in vivo* using DLBCL tumor-bearing mouse models. MiR-429 and FOXO1 expression levels were downregulated, whereas DNMT3A was upregulated in DLBCL compared to the control group. PA treatment was associated with enhanced autophagy, mediated by the upregulation of miR-429 and downregulation of DNMT3A. The luciferase reporter assay and MSP confirmed that miR-429 directly inhibits DNMT3A, thereby reducing FOXO1 methylation. Subsequent experiments demonstrated that PA promotes autophagy and inhibits DLBCL progression by upregulating miR-429 and modulating the DNMT3A/FOXO1 axis. *In vivo* PA significantly reduced the growth of xenografted tumors through its regulatory impact on the miR-429/DNMT3A/FOXO1 axis. Palmitic acid may modulate autophagy and inhibit DLBCL progression by targeting the miR-429/DNMT3A/FOXO1 signaling pathway, suggesting a novel therapeutic target for DLBCL management.

[KEY WORDS] Palmitic acid; Diffuse large B-cell lymphoma; MiR-429; DNMT3A; FOXO1; Autophagy
[CLC Number] R965 **[Document code]** A **[Article ID]** 2095-6975(2024)06-0554-14

Introduction

Diffuse large B-cell lymphoma (DLBCL) is the most prevalent form of non-Hodgkin's lymphoma (NHL), comprising approximately 30% of all NHL cases [1]. Diagnosis of DLBCL necessitates specialized testing methods such as immunohistochemistry, flow cytometry, and molecular assays, which are typically conducted by an expert hematopathologist [1]. Recent therapeutic advancements have introduced several agents, including Polatuzumab vedotin combined with bendamustine and rituximab, selinexor, and tafasitamab plus lenalidomide [1, 2]. DLBCL is notably phenotypically and genetically diverse. Research has identified crucial genetic mutations in genes such as MCD, BN2, N1, and EZB that significantly contribute to the pathogenesis of DLBCL [3]. Owing to its diverse etiologies, approximately 40% of patients suffer from disease refractoriness or relapse [4], underscoring the urgency to decipher the underlying mechanisms of DLBCL pathogenesis and drug resistance to enhance clinical outcomes. Palmitic Acid (PA), a primary free fatty acid

[Received on] 28-Nov.-2023
[Research funding] This work was supported by Henan Province Science and Technology Research and Development in 2023 (Guiding Project Approval): Study on the role and mechanism of Xiakucao extract in regulating autophagy therapy for diffuse large B-cell lymphoma through the PI3K/AKT signaling pathway (No. 232102310451) and Henan Province Traditional Chinese Medicine Top Talents Project: Study on the effect and mechanism of Xiakucao extract on diffuse large B-cell lymphoma (No. 2022ZYBJ18).
[*Corresponding author] E-mail: zhangmingzhi2z518@163.com
These authors have no conflict of interest to declare.

(FFA) in human plasma and the predominant saturated fatty acid (SFA) in membrane phospholipids [5], has been increasingly reported to inhibit cancer cell proliferation, metastasis [6], and invasive motility [7, 8]. Recent studies have demonstrated that PA can elevate LC3 expression by activating the c-Jun *N*-terminal kinase (JNK) signaling pathway [9]. Moreover, another study reported that PA significantly increased the release of intracellular reactive oxygen species (ROS) and induced damage to mitochondrial membranes in human lymphoma cells [10], suggesting that PA may play a role in modulating lymphoma development. Despite these insights, there is a scarcity of comprehensive reports on the mechanisms and potential roles of PA in DLBCL pathogenesis, highlighting a significant gap in the current understanding and treatment of this disease.

MicroRNAs (miRNAs) are short noncoding RNAs that bind specifically to the 3′-untranslated region (UTR) of their target mRNAs, leading to gene silencing or inhibition of translation [11]. Recent studies have identified several miRNAs, such as exosomal miR-99a-5p and miR-125b-5p, as potential biomarkers for DLBCL [12]. MiR-429, in particular, has demonstrated antitumor effects in various cancers, including breast cancer [13], pancreatic cancer [14], and lymphoma [15, 16]. One study highlighted that miR-429 was upregulated in marginal zone lymphoma (MALT) [15], and another revealed that miR-429 targets chromobox 8 (CBX8), leading to decreased CBX8 expression and enhanced apoptosis in DLBCL. However, a comprehensive understanding of how miR-429 regulates DLBCL progression remains limited. Consequently, targeting miR-429 presents a novel approach to exploring the mechanisms underlying DLBCL development, potentially offering new avenues for therapeutic intervention.

DNA methylation is a well-characterized epigenetic modification that plays a crucial role in various biological processes, including cellular development, differentiation, gene expression, genomic imprinting, and X-chromosome inactivation [17]. Previous studies have highlighted aberrant methylation at specific gene loci, such as the INK4b-ARF-INK4a locus, as a significant epigenetic anomaly in DLBCLs, closely linked to clinical outcomes [18]. Genomic analyses of DLBCL have shown that DNA methyltransferase 3A (DNMT3A) is actively involved in the epigenetic alterations observed in this disease [19]. DNMT3A catalyzes the methylation of cytosine residues within CpG islands (CGIs) in gene promoters, effectively silencing gene transcription. This aberration in DNMT3A function is considered an early event in the development of DLBCL [20]. Observations from a study on primary gastrointestinal diffuse large B-cell lymphoma (PGI-DLBCL) indicate that lower levels of DNMT3A correlate with improved survival outcomes [21], underscoring its critical role in DLBCL pathophysiology. Utilizing the StarBase online bioinformatics tool (https://starbase.sysu.edu.cn/), we identified a potential binding sequence for miR-429 within DNMT3A. Furthermore, existing research has demonstrated that miR-429 can target the 3′-UTR of DNMT3A in prostate cancer [22]. However, the interaction between miR-429 and DNMT3A in DLBCL remains unexplored. DNMT3A is part of a family that includes DNMT1, DNMT2, and DNMT3 [23]. Additional bioinformatics analysis revealed that the promoter region of Forkhead box protein O1 (FOXO1) contains a CGI, suggesting a potential regulatory mechanism involving DNMT3A; however, the specific interactions between DNMT3A and FOXO1 in this context have not yet been reported.

In this study, we hypothesized that PA could elevate miR-429 levels, subsequently suppressing DNMT3A expression in DLBCL. This suppression is posited to enhance FOXO1-modulated autophagy, thereby inhibiting DLBCL progression. The aim of our research is to elucidate the novel molecular mechanisms through which PA exerts its therapeutic effects in DLBCL, potentially providing a basis for improved treatment strategies.

Materials and Methods

DLBCL tumor tissues and normal tissues from patients

Specimens of DLBCL tumor lymph nodes were obtained from 30 patients diagnosed with DLBCL (n = 30). Correspondingly, normal lymph node samples were collected from 30 non-cancer patients undergoing lymph node biopsies. All sample collections were performed at the Affiliated Hospital of Zhengzhou Medical University. The study protocol received approval from the ethics committee of the Affiliated Hospital of Zhengzhou Medical University, and informed consent was obtained from all participants. The median age of the patients with DLBCL was 51 years (range: 42–76 years), while the median age of the control group was 49 years (range: 45–81 years). Detailed clinical characteristics, including clinical stage, histological type, and pathological grading of the patients, were systematically recorded in a dedicated database.

Bioinformatics analysis

The online software StarBase 2.0 (http://starbase.sysu.edu.cn/) was used to predict the potential binding site between miR-429 and DNMT3A.

Cell culture

The female lymphoblastoid cell line GM12878 was obtained from the Coriell Institute for Medical Research, Camden, New Jersey, USA (Coriell Institute). (https://www.coriell.org/0/Sections/Search/Sample_Detail.aspx?Ref=GM12878&Product=CC). DLBCL cell lines OCI-Ly10 (CVCL_8795), SU-DHL-4 (CVCL_0539), OCI-Ly7 (CVCL_1881), and Farage (CVCL_3302) were acquired from Cellosaurus (Lausanne, Switzerland).These cells were cultured in RPMI 1640 medium (11875119, Thermo Fisher Scientific, CA, USA) supplemented with 2 mmol·L^{-1} L-glutamine (A29168-01, Thermo Fisher Scientific, CA, USA), 15% fetal bovine serum, and 100 U·mL^{-1} penicillin-streptomycin (15140148, Thermo Fisher Scientific, CA, USA). Cultures were maintained at 37 °C in a humidified atmosphere containing 5% CO_2 condition. The medium was refreshed every 2–3 days, and cells were passaged upon reaching 80%–90% confluency.

Cell transfection

MiR-429 mimics and inhibitors, along with their respective control NC mimics and NC inhibitors, were procured from GenaPharma, Shanghai, China. The overexpression plasmid for pCMV6-DNMT3A (RC208192) and its corresponding empty control vector, pCMV6, were sourced from OriGene Technologies, Inc., Rockville, MD, USA. For transfection, Lipofectamine 3000 reagent (L3000015, Thermo Fisher Scientific, CA, USA) was employed. Scientific, CA, USA). Cells were collected 48 h post-transfection, and the transfection efficiency was assessed using RT-qPCR.

Xenograft tumor model

OCI-Ly7 cells were dissociated and counted following harvesting. A total of 1×10^7 OCI-Ly7 cells were resuspended in 300 μL of sterile Phosphate Buffered Saline (PBS) and injected subcutaneously into the right flank region of 4-week-old male BALB/c nude mice (obtained from Guangdong Medical Laboratory Animal Center, Guangdong, China). Post-injection, mice were treated with 200 $mg \cdot kg^{-1}$ of PA three times per week for two weeks. Tumor volumes were measured five days post-injection and subsequently at specified intervals. At the end of four weeks, the mice were euthanized using carbon dioxide, and the tumors were excised and weighed. The excised tumors were then fixed in formalin, embedded in paraffin wax, and sectioned. Immunohistochemical (IHC) analyses were performed on the tumor sections to determine the expression levels of DNMT3A and FOXO1. The animal study protocols were approved by the Ethics Committee of the Affiliated Hospital of Zhengzhou Medical University.

Luciferase reporter assay

The potential binding site of miR-429 in DNMT3A was predicted using StarBase online software (http://starbase.sysu.edu.cn/). Wild-type (WT) and mutated (MUT) versions of DNMT3A were cloned into the pGL-CMV luciferase reporter plasmid, which contains both wild-type and mutant potential binding sequences for miR-429. The luciferase reporter plasmids were transfected into cells using Lipofectamine 3000 (L3000015, Thermo Fisher Scientific, CA, USA) according to the manufacturer's instructions. Luciferase activity was measured 48 h post-transfection using a commercial reporter assay kit (E1910, Promega, WI, USA).

Methylation-specific PCR

A 50 $mmol \cdot L^{-1}$ stock solution of 5-Azacytidine (5-Aza, A2385, Sigma-Aldrich, MO, USA) was prepared in DMSO and stored at -80°C until use. Cells were treated with 1 μM 5-Aza or an equivalent volume of DMSO, or they were transfected with either sh-NC or shRNA against DNMT3A (sh-DNMT3A) using Lipofectamine 3000 (L3000015, Thermo Fisher Scientific, CA, USA). After 72 h, cells were harvested, and total RNA was extracted using Trizol reagent (T9424, Sigma-Aldrich, MO, USA). Methylation levels were assessed using the Bisulfite Conversion Kit (K1461) and DNA Methylation Analysis Kit (K1441) from Thermo Fisher Scientific, CA, USA, following the manufacturer's detailed instructions. Primers for the unmethylated reaction were forward 5′-TCGTCATAATCTGTCCCTACACA-3′ and reverse 5′-CGGCTTCGGCTCTTAGCAAA-3′. For the methylation reaction, the primers were forward 5′-GTTTAATTTA-GAGGGTGGTAAGAGC-3′ and reverse 5′-CTTTCTTCT-TAACAACTCGACTTCG-3′. The Polymerase chain reaction (PCR) products were visualized on a 1.5% agarose gel. Expected sequences for unmethylated and methylated FOXO1 are detailed in Table 1.

Table 1 The expected PCR product and the nucleotide sequence within the FoxO1 promoter.

Name	Specific sequences
The expected PCR sequence (−572/−273)	5′-GAAAACATTAAACCAAAACAAAACCCACCGATTCCCCACGTCGTTCAGCAAAGACATCGTGGGT GGAGCCAGGAGGGAGCGATTGAGTAGAATTCCTCGCGGCCGCCTCCGCCCGCCCACCCCGCGCCCC CGGCCCTCGGCCCCCTGCCCTGCCAGCCCGCCGGGCTCGGCCCGCAGCGGAGGTCAGGGAGCAGCG AGCGCCTCCTCCCACCCGGGCTTCCCGAGTACTCGGCTCTGCTGCTCCGTAGTAAACAAAGTGTCGC CGGCGCCTCCACGCTGGTTTGCTTCCTAGCAATCAAA-3′
The sequences of methylated FoxO1	5′-GAAAATATTAAATTAAAATAAAATTTATCGATTTTTTACGTCGTTTAGTAAAGATATCGTGGGTG GAGTTAGGAGGGAGCGATTGAGTAGAATTTTTCGCGGTCGTTTTCGTTCGTTTATTTCGCGTTTTCGG TTTTCGGTTTTTTGTTTTGTTAGTTCGTCGGGTTCGGTTCGTAGCGGAGGTTAGGGAGTAGCGAGCGT TTTTTTTTATTCGGGTTTTTCGAGTATTCGGTTTTGTTGTTTCGTAGTAAATAAAGTGTCGTCGGCGTT TTTACGTTGGTTTGTTTTTTAGTAATTAAA-3′

Immunohistochemistry

For immunohistochemistry, rabbit anti-DNMT3A (1 : 1000, ab188470) and rabbit anti-FOXO1 (1 : 250, ab52857) antibodies were purchased from Abcam, Inc., MA, USA. Immunostaining was performed using a DAB substrate kit (ab64238, Abcam, Inc., MA, USA) and counterstained with hematoxylin solution (ab220365, Abcam, Inc., MA, USA). Images of the stained samples were captured using an inverted Nikon Eclipse TE2000-U Inverted Fluorescence Microscope (TE2000-U, New York, USA).

MTS and Flow cytometry assays

SU-DHL-4 and OCI-Ly7 cells were treated for 24 h with either vehicle, PA, or a combination of PA with NC inhibitor, miR-429 inhibitor, overexpression control (oe-NC), overexpression vector for DNMT3A (oe-DNMT3A), shRNA negative control (sh-NC), sh-DNMT3A, or miR-429 inhibitor + sh-DNMT3A. Post-treatment, cells were harvested to assess cell viability and mortality. Cell viability was determined using a commercial Cell Proliferation Assay kit (G3582, Promega Corporation, WI, USA). Cell mortality was analyzed using a FITC Annexin V Apoptosis Detection Kit with PI (640914, Biolegend, CA, USA), and the analysis was conducted on a BD FACSAria™ III flow cytometer (BD FACSAria III, BD Bioscience, USA) following the manufacturer's detailed in-

structions.

TUNEL assay

Tumor sections were dewaxed, rehydrated, and rinsed in distilled water. The sections were then treated with 5% hydrogen peroxide for 10 min to inactivate endogenous peroxidases, followed by three washes with 1 × DPBS. Apoptotic cells were detected using commercial TUNEL Assay Kits (C10617, Thermo Fisher Scientific, CA, USA). Nuclei were stained with DAPI (1 : 2000, 62248, Thermo Fisher Scientific, CA, USA). Images of the sections were captured using an EVOS™ M5000 Imaging System (AMF5000, Thermo Fisher Scientific, CA, USA).

RT-qPCR

Total RNA was extracted using RNeasy Kits (74004, Qiagen, MD, USA). One microgram of total RNA was used for cDNA synthesis using the High-Capacity cDNA Reverse Transcription Kit (4368813, Thermo Fisher Scientific, CA, USA). Subsequently, RT-qPCR was conducted using an RT-qPCR SYBR Green ROX Kit on QuantStudio™ 3 Real-Time PCR System (A28136, Thermo Fisher Scientific, CA, USA). The PCR primers used were as follows: miR-429 forward 5′-TACTGTCTGGTAAAACCG-3′ and reverse 5′-GAACATGTCTGCGTATCTC-3′; U6 forward 5′-CTCGCTTCGGCAGCACAT-3′ and reverse 5′-TTTGCGTGTCATCCTTGCG-3′; DNMT3A forward 5′-CCTCTTCGTTGGAGGAATGTGC-3′ and reverse 5′-GTTTCCGCACATGAGCACCTCA-3′; FOXO1 forward 5′-CTACGAGTGGATGGTCAAGAGC-3′ and reverse 5′-CCAGTTCCTTCATTCTGCACACG-3′; GAPDH forward 5′-GTCTCCTCTGACTTCAACAGCG-3′ and reverse 5′-ACCACCCTGTTGCTGTAGCCAA-3′. Relative gene expression levels were determined using the $2^{-\Delta\Delta CT}$ method.

Western blotting assay

Total proteins were extracted from DLBCL cell lines or xenografted tumor tissues using Radio-Immunoprecipitation Assay (RIPA) buffer (ab156034, Abcam, Inc., MA, USA) supplemented with the protease inhibitor PMSF (ab141032, Abcam, Inc., MA, USA). Protein concentrations were measured using a BCA protein assay kit (ab102536, Abcam, Inc., MA, USA). 10 μg of total proteins were separated by 10% sodium dodecyl sulfate-polyacrylamide gel electrophoresis (SDS-PAGE) and transferred to the nitrocellulose membrane. The membranes were washed briefly with 1 × PBST (PBS with 0.05% Tween® 20), blocked with 5% non-fat milk in 1 × PBST for 1 h at room temperature, and incubated overnight at 4 °C with primary antibodies. Primary antibodies used were rabbit anti-mTOR (1 : 2000, ab32028, Abcam, Inc., MA, USA), rabbit anti-mTOR (phospho S2448) antibody (1 : 2000, ab131538, Abcam, Inc., MA, USA), rabbit anti-LC3I/II (1 : 2000, ABC929, Sigma-Aldrich, MO, USA), rabbit anti-p62 (1 : 2000, ab91526, Abcam, Inc., MA, USA), and mouse anti-β-actin (1 : 2000, ab6276, Abcam, Inc., MA, USA) as the loading control. Following incubation, membranes were washed three times with 1 × PBST and incubated with corresponding secondary antibodies: goat anti-rabbit IgG H&L (HRP) (1 : 2000, ab205718, Abcam, Inc., MA, USA) and goat anti-mouse IgG H&L (HRP) (1 : 2000, ab6789, Abcam, Inc., MA, USA) for 2 h at room temperature. After three further washes, the proteins were visualized using an ECL kit (ab133406, Abcam, Inc., MA, USA) and imaged with Image Lab 3.0 (17006130, Bio-Rad Laboratories, Inc, CA, USA).

Statistical analysis

All data were expressed as means ± standard deviation (Mean ± SD). Experiments were independently repeated at least three times. The statistical analyses were conducted using Prism GraphPad 9. The differences were analyzed by Student's *t*-test or way ANOVA of variance with the *post hoc Tukey test.* The differences among groups were considered significant at $P < 0.05$.

Results

MiR-429 and FOXO1 were downregulated, and DNMT3A was upregulated in DLBCL.

To investigate the potential roles of miR-429, FOXO1, and DNMT3A in the development of DLBCL, we assessed their expression in DLBCL tumor tissues and cell lines using RT-qPCR and Western blotting assays. The results indicated that miR-429 and FOXO1 were consistently downregulated, whereas DNMT3A was upregulated in DLBCL tissues compared to normal control tissues (Figs. 1A–1C). Similar trends were observed in DLBCL cell lines (SU-DHL-4, OCI-Ly7, OCI-Ly10, and Farage), where miR-429 and FOXO1 levels were significantly lower, and DNMT3A levels were markedly higher than in the normal lymphoblastoid cell line GM12878 (Figs. 1D–1F), particularly in SU-DHL-4 and OCI-Ly7 cells. Additionally, protein analyses confirmed that DNMT3A levels were elevated, and FOXO1 levels were reduced in these cell lines, especially in SU-DHL-4 and OCI-Ly7 (Fig. 1G). These findings suggest a pattern of reduced miR-429 and FOXO1 expression, coupled with increased DNMT3A expression, in DLBCL.

PA (25–100 μmol·L^{-1}) enhanced miR-429 expression to influence the phenotype of DLBCL.

We further investigated whether PA at varying concentrations (25–100 μmol·L^{-1}) affected the expression of miR-429 and its role in the progression of DLBCL. Our findings demonstrated that PA increased miR-429 expression in DLBCL cell lines SU-DHL-4 and OCI-Ly7 in a dose-dependent manner (Fig. 2A). However, they dramatically decreased cell viability in a dose-dependent manner (Fig. 2B). Concurrently, PA significantly reduced cell viability in these cell lines, also in a dose-dependent fashion (Fig. 2B), and elevated levels of cell mortality (Fig. 2C). Notably, at a concentration of 50 μmol·L^{-1}, PA notably augmented miR-429 expression and cell mortality, while reducing cell viability compared to the control group (Figs. 2A–2C). Further analysis using immunofluorescent staining revealed that PA, compared to the control, significantly increased autophagic flux in both SU-DHL-4 and OCI-Ly7 cells. The application of Bafilomycin A1 (BafA1), a known autophagy inhibitor, substantially reduced

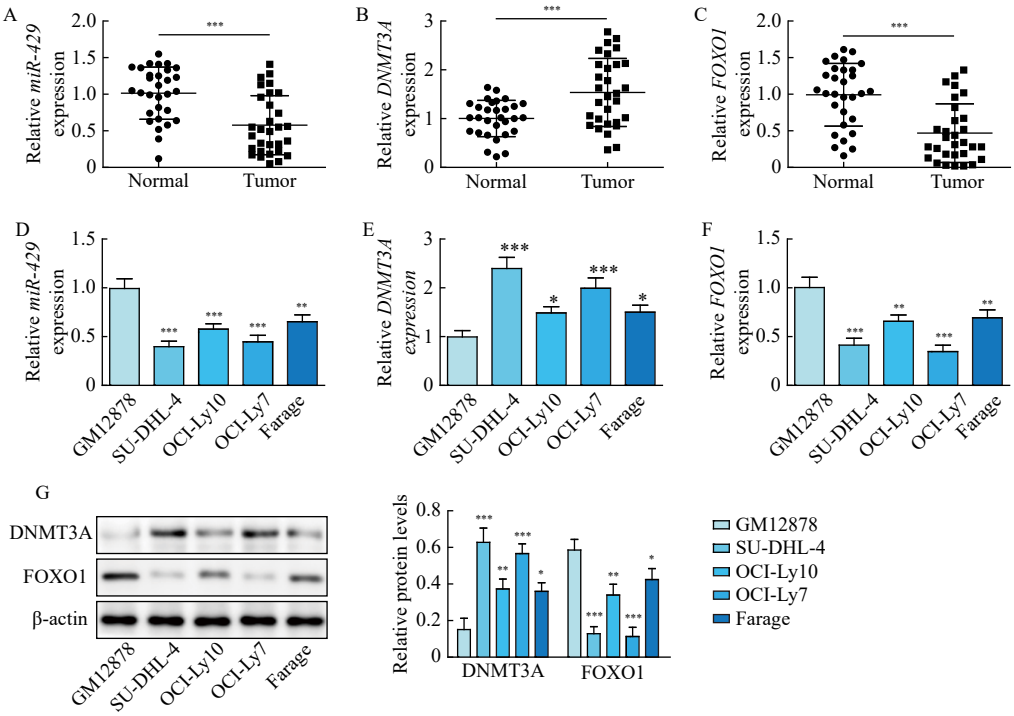

Fig. 1 *miR-429* and *FOXO1* were downregulated, and *DNMT3A* was upregulated in DLBCL. (A–C) The expressions of *miR-429*, *DNMT3A*, and *FOXO1* were detected by RT-qPCR in tumor tissues from patients with DLBCL and normal lymph node tissues. (D–F) The expressions of *miR-429*, *DNMT3A*, and *FOXO1* were detected by RT-qPCR in normal lymphoblastoid cell GM12878 and four DLBCL cell lines (SU-DHL-4, OCI-Ly7, OCI-Ly10, and Farage). (G) The protein levels of DNMT3A and FOXO1 were determined by Western blotting assay in normal lymphoblastoid cell GM12878 and four DLBCL cell lines. Data are representative of three independent experiments ($n = 30$). $^{*}P < 0.05$, $^{**}P < 0.01$, $^{***}P < 0.001$ *vs* the corresponding control.

the formation of autophagosomes and attenuated the PA-induced autophagic activity (Fig. 2D). Based on these results, PA at 50 μmol·L^{-1} was selected for subsequent experiments. Additional Western blotting analysis showed that PA markedly downregulated mTOR (ser2448) and p62 expressions and facilitated the conversion of LC3I to LC3II, indicating an enhancement in autophagy in DLBCL cells. The autophagy inhibitor BafA1 mitigated the PA-induced autophagy effects (Fig. 2E). These findings suggest that PA enhances the expression of miR-429, which in turn regulates autophagy in DLBCL cells, underscoring the therapeutic potential of targeting autophagy in DLBCL treatment.

PA enhanced autophagy by upregulating miR-429.

To explore the effects of PA-upregulated miR-429 upregulation on cell autophagy, we first evaluated the transfection efficiency of NC inhibitor and miR-429 inhibitor. The results confirmed that the transfection of miR-429 inhibitor for 24 h significantly reduced miR-429 levels in both SU-DHL-4 and OCI-Ly7 cells (Fig. 3A). Furthermore, the miR-429 inhibitor notably reduced the elevated miR-429 levels induced by PA exposure (Fig. 3B). Subsequent assays involving MTS and flow cytometry revealed that PA exposure significantly decreased cell viability and increased cell mortality. Intriguingly, the miR-429 inhibitor mitigated the PA-induced decrease in cell viability and elevation in cell mortality (Figs. 3C–3D). Additional immunofluorescent staining indicated that the NC inhibitor did not reverse the high autophagic flux induced by PA. However, the miR-429 inhibitor substantially reduced the autophagic flux in both SU-DHL-4 and OCI-Ly7 cells (Fig. 3E). As shown in Fig. 3F, PA treatment significantly decreased the phosphorylation levels of mTOR at the Ser2448 site and p62 protein levels, while increasing the LC3II/LC3I ratio, which indicates enhanced autophagy. Conversely, the miR-429 inhibitor increased the phosphorylation of mTOR and p62 levels and decreased the LC3II/LC3I ratio, indicating a suppression of autophagy. In summary, our findings suggest that PA promotes autophagy and apoptosis in SU-DHL-4 and OCI-Ly7 cells by upregulating miR-429. This mechanistic insight reveals a pivotal role of miR-429 in modulating the autophagic pathways influenced by PA, providing a potential therapeutic target for DLBCL treatment.

PA enhanced autophagy by inhibiting DNMT3A expression.

To elucidate the mechanism by which PA enhances cell autophagy, we assessed the expression of DNMT3A in cells treated with and without PA. Following the transfection with either an oe-NC or an oe-DNMT3A, we observed a significant increase in DNMT3A mRNA levels with oe-DNMT3A compared to oe-NC (Fig. 4A). PA treatment led to a reduction in DNMT3A expression relative to the vehicle control. However, DNMT3A overexpression *via* oe-DNMT3A transfection substantially counteracted the PA-induced reduction in DNMT3A levels (Fig. 4B). Moreover, DNMT3A overexpression significantly mitigated the cytotoxic effects induced

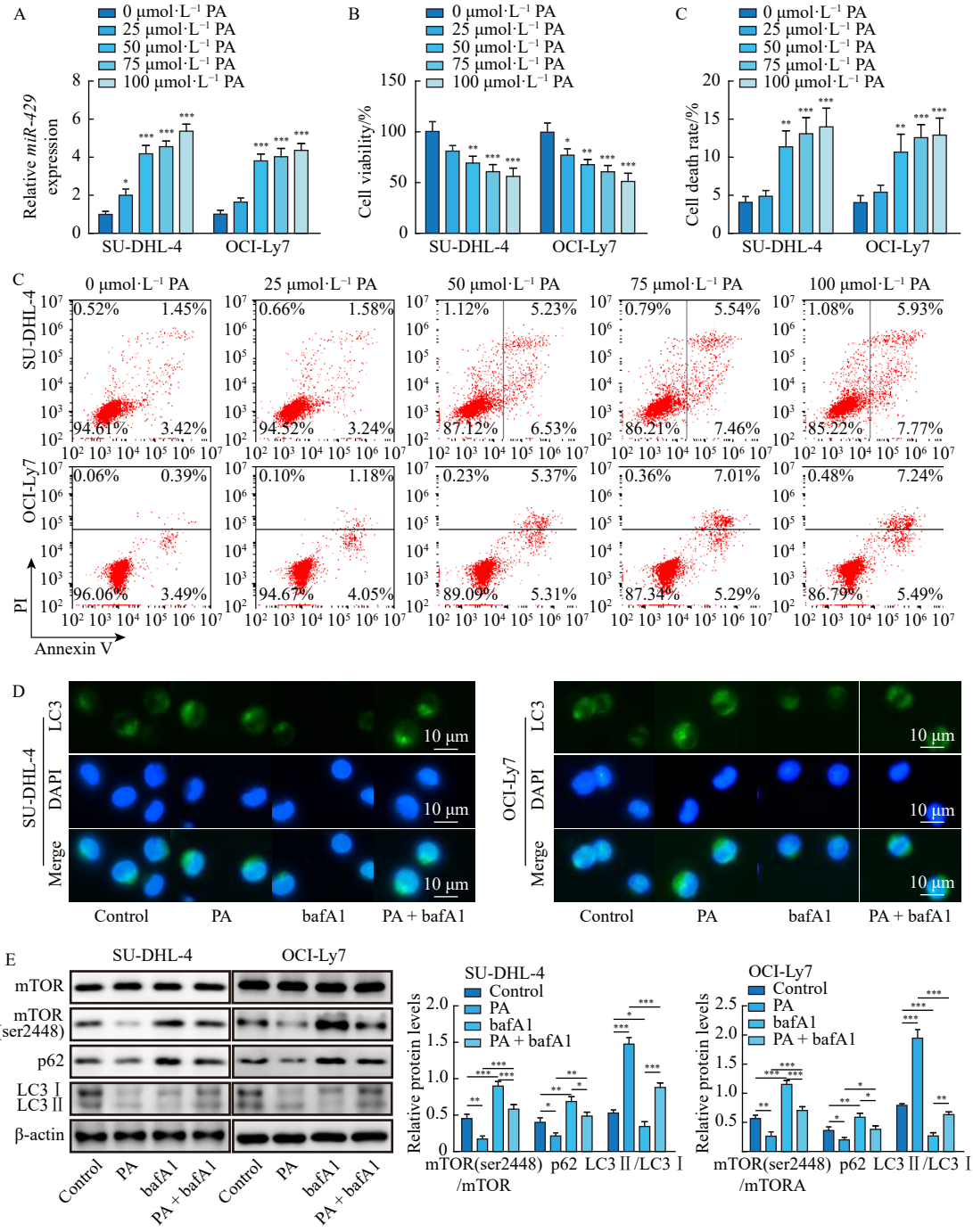

Fig. 2 PA (25-100 μmol·L^{-1}) enhanced miR-429 expression to influence the phenotype of diffuse large B-cell lymphoma. A. The miR-429 levels were assayed by RT-qPCR in DLBCL cell lines SU-DHL-4 and OCI-Ly7 after treatment by vehicle or PA (25–100 μmol·L^{-1}) for 24 h. B. Cell viabilities were assessed by MTS assay in DLBCL cell lines. C. Dead cells were measured by flow cytometry assay in DLBCL cell lines. D. The autophagic flux was detected by immunofluorescent staining using the autophagy-specific antibody LC3 in both SU-DHL-4 and OCI-Ly7 cells after the treatment with control, PA, bafA1, or PA + bafA1. Scale bar = 10 μm. E. The protein levels of mTOR, mTOR(ser2448), p62, and LC3II/I were detected by Western blotting assay in DLBCL cell lines SU-DHL-4 and OCI-Ly7 after treatment by vehicle, PA (50 μmol·L^{-1}), or PA + bafA1 (50 μmol·L^{-1}) for 24 h. Data are representative of three independent experiments. $^{*}P < 0.05$, $^{**}P < 0.01$, $^{***}P < 0.001$ *vs* the corresponding control.

by PA compared with oe-NC transfection (Figs. 4C–4D). An autophagic flux assay revealed that while oe-NC did not inhibit autophagic flux relative to PA treatment, oe-DNMT3A markedly suppressed the increased autophagic flux induced by PA in both SU-DHL-4 and OCI-Ly7 cells (Fig. 4E). Western blotting analysis further demonstrated that DNMT3A overexpression enhanced the phosphorylation of mTOR at ser2448 and increased p62 expression, while reducing the ra-

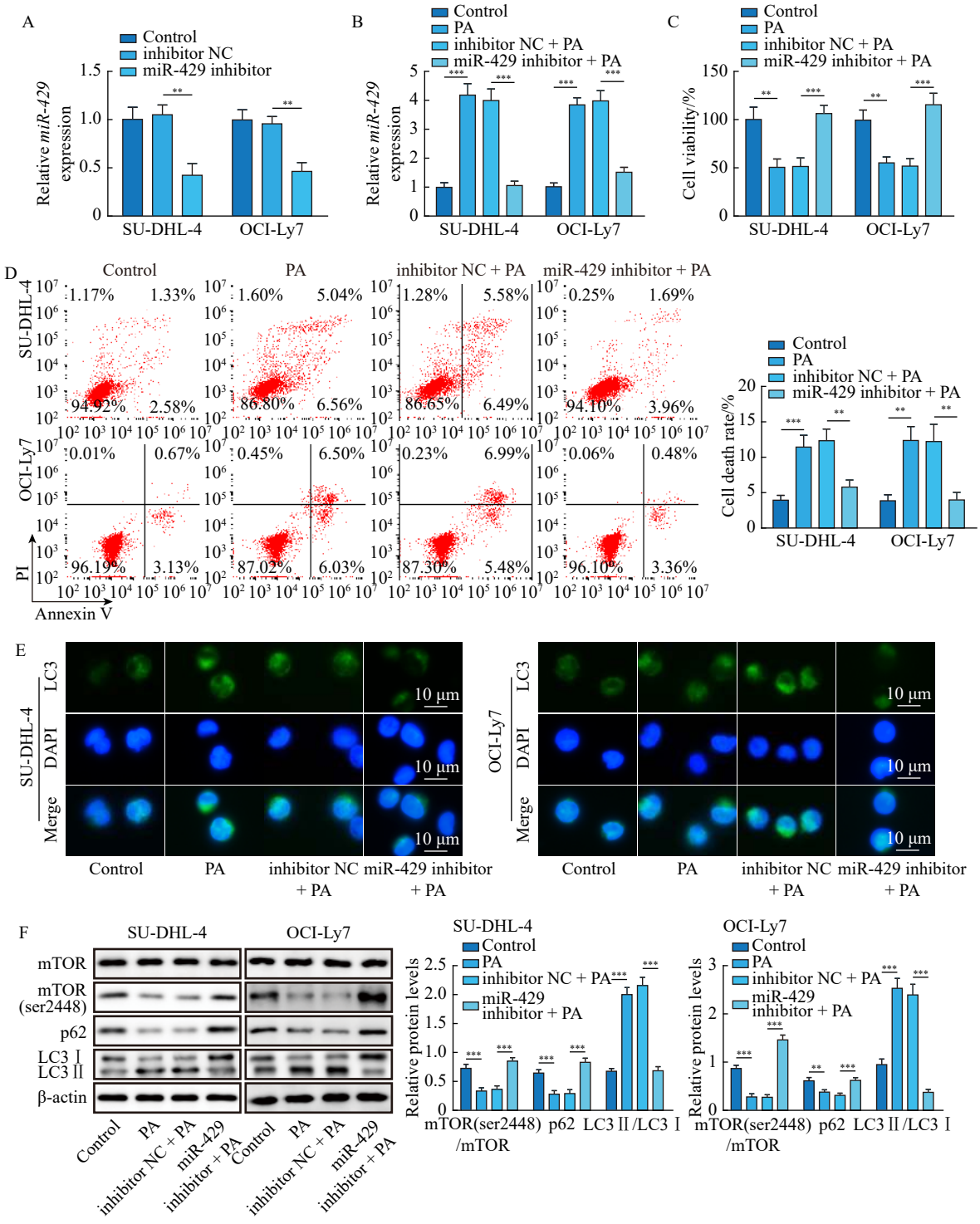

Fig. 3 PA enhanced autophagy by upregulating miR-429. A. The transfection efficiencies were determined by RT-qPCR in DLBCL cell lines SU-DHL-4 and OCI-Ly7 after NC inhibitor and miR-429 inhibitor transfection for 24 h. B. The miR-429 levels were detected by RT-qPCR in DLBCL cell lines SU-DHL-4 and OCI-Ly7 after treatment by vehicle, PA (50 μmol·L^{-1}), PA + NC inhibitor or PA + miR-429 inhibitor for 24 h. C. Cell viabilities were analyzed by MTS assay in DLBCL cell lines SU-DHL-4 and OCI-Ly7 after the transfection of NC inhibitor and miR-429 inhibitor for 24 h, followed by the treatment with vehicle or 50 μmol·L^{-1} PA. D. Cell mortality was detected by flow cytometry assay in DLBCL cell lines SU-DHL-4 and OCI-Ly7. E. The autophagic flux was detected by immunofluorescent staining using the autophagy-specific antibody LC3 in both SU-DHL-4 and OCI-Ly7 cells after the treatment with control, PA, inhibitor NC + PA or miR-429 inhibitor + PA. Scale bar = 10 μm. F. The protein levels of mTOR, mTOR(ser2448), p62, and LC3II/I were detected by Western blotting assay in DLBCL cell lines. Data are representative of three independent experiments. $^{**}P < 0.01$, $^{***}P < 0.001$ *vs* the corresponding control.

tio of LC3II to LC3I under PA treatment (Fig. 4F). These results suggest that PA promotes cell autophagy by downregulating DNMT3A, which in turn decreases the phosphorylation of mTOR and p62 expression but increases the conversion of LC3-I to LC3-II —an indicator of autophagosome formation (Fig. 4F). Conversely, DNMT3A overexpression can significantly counteract the autophagy-enhancing effects of PA, highlighting DNMT3A's critical role in regulating

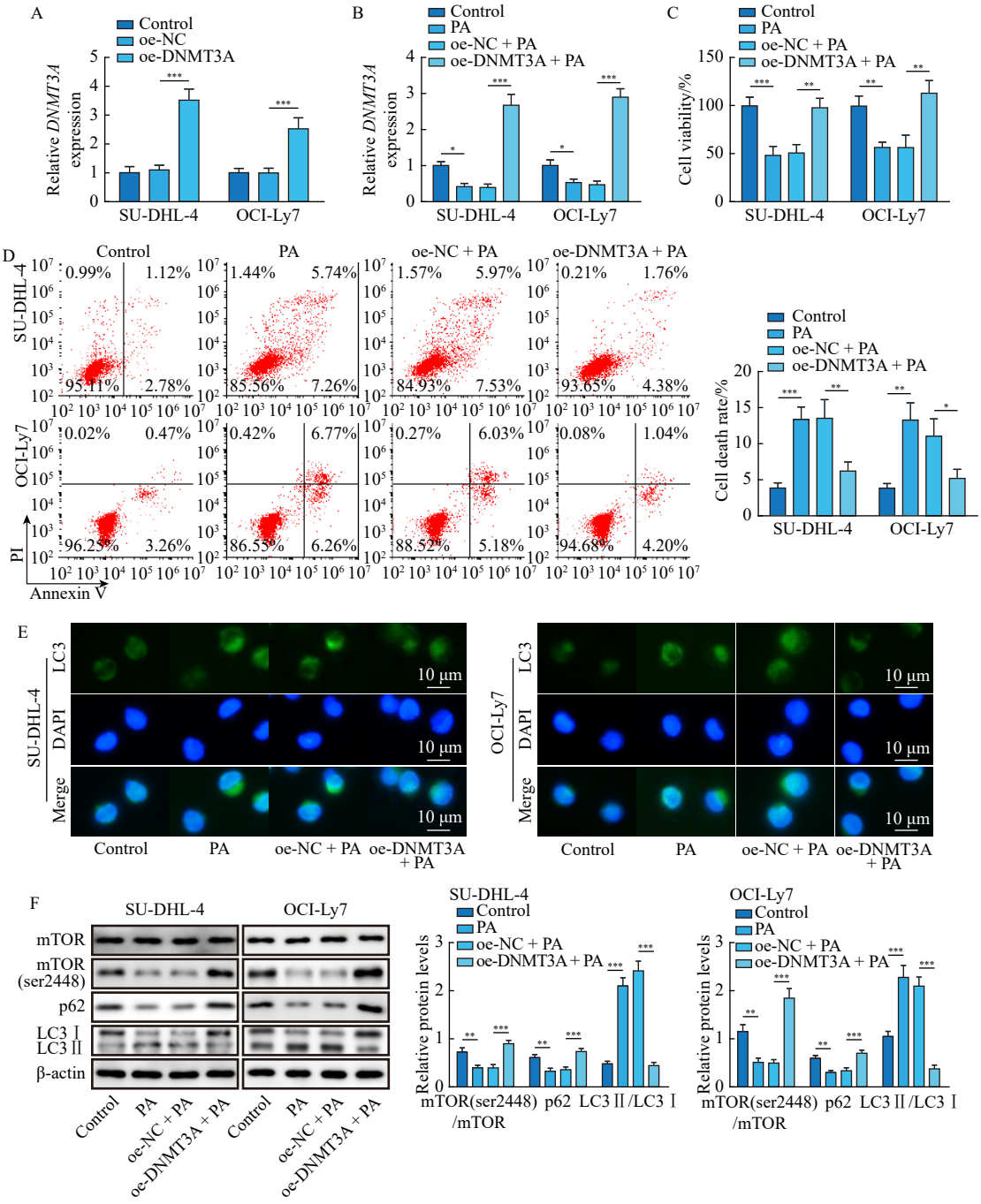

Fig. 4 PA enhanced cell autophagy by inhibiting DNMT3A expression. A. The transfection efficiencies were determined by RT-qPCR in DLBCL cell lines SU-DHL-4 and OCI-Ly7 after the transfection of oe-NC or oe-DNMT3A. B. RT-qPCR detected the expression of DNMT3A in DLBCL cell lines SU-DHL-4 and OCI-Ly7 after the transfection of oe-NC or oe-DNMT3A, followed by the treatment with vehicle or 50 μmol·L^{-1} PA. C. MTS assays measured cell viability in DLBCL cell lines. D. Flow cytometry evaluated the cell mortality in DLBCL cell lines. E. The autophagic flux was detected by immunofluorescent staining using the autophagy-specific antibody LC3 in both SU-DHL-4 and OCI-Ly7 cells after the treatment with control, PA, oe-NC + PA or oe-DNMT3A + PA. Scale bar = 10 μm. F. The protein levels of mTOR, mTOR (ser2448), p62, and LC3II/I were measured by Western blotting assay in DLBCL cell lines SU-DHL-4 and OCI-Ly7. Data are representative of three independent experiments. $^{*}P < 0.05$, $^{**}P < 0.01$, $^{***}P < 0.001$ *vs* the corresponding control.

autophagy in DLBCL cells.

MiR-429 regulated FOXO1 expression by directly binding to DNMT3A.

To explore the hypothesis that miR-429 modulates DNMT3A expression and thereby influences PA-induced autophagy in DLBCL, we transfected SU-DHL-4 and OCI-Ly7 cells with NC mimics and miR-429 mimics and then measured DNMT3A expression. RT-qPCR results confirmed that miR-429 mimics significantly decreased DNMT3A levels (Fig. 5A). Using the online tool StarBase (http://starbase.sysu.edu.cn/), we predicted a potential miR-429 binding site on the DNMT3A sequence, with the alignment illustrated in (Fig. 5B). Luciferase reporter assays further validated this interaction, showing that miR-429 mimics inhibited luciferase activity in cells transfected with the WT DNMT3A construct but not with the MUT DNMT3A construct (Fig. 5C). Western blotting analysis revealed that DNMT3A knockdown significantly increased FOXO1 expression (Fig. 5D). Thus, we investigated whether miR-429-altered DNMT3A expression was associated with the methylation status of the FOXO1 promoter in DLBCL. Then we conducted the biochemical analysis to examine the methylation level of the FOXO1 promoter. The FOXO1 promoter region contained CpG islands (CGIs) in the FOXO1 promoter region, as shown in Fig. 5E. Methylation-specific PCR was conducted on samples treated with DMSO or 5-Azacytidine (5Aza), a DNA methylation inhibitor, and transfected with either sh-NC or sh-DNMT3A. As expected, 5Aza treatment markedly reduced the methylation status of the FOXO1 promoter compared to DMSO (Fig. 5F), and DNMT3A knockdown also led to a significant decrease in FOXO1 methylation(Fig. 5F). These results confirm that miR-429 promotes autophagy by directly silencing DNMT3A, thus upregulating FOXO1 expression. Additional investigations into whether DNMT3A regulates miR-429 showed that DNMT3A knockdown significantly increased miR-429 expression, our results in Fig. S1A. In Fig. S1B, we predicted the status of miR-429 promoter (−2000/+100 bp). Predictive analysis of the miR-429 promoter region identi-

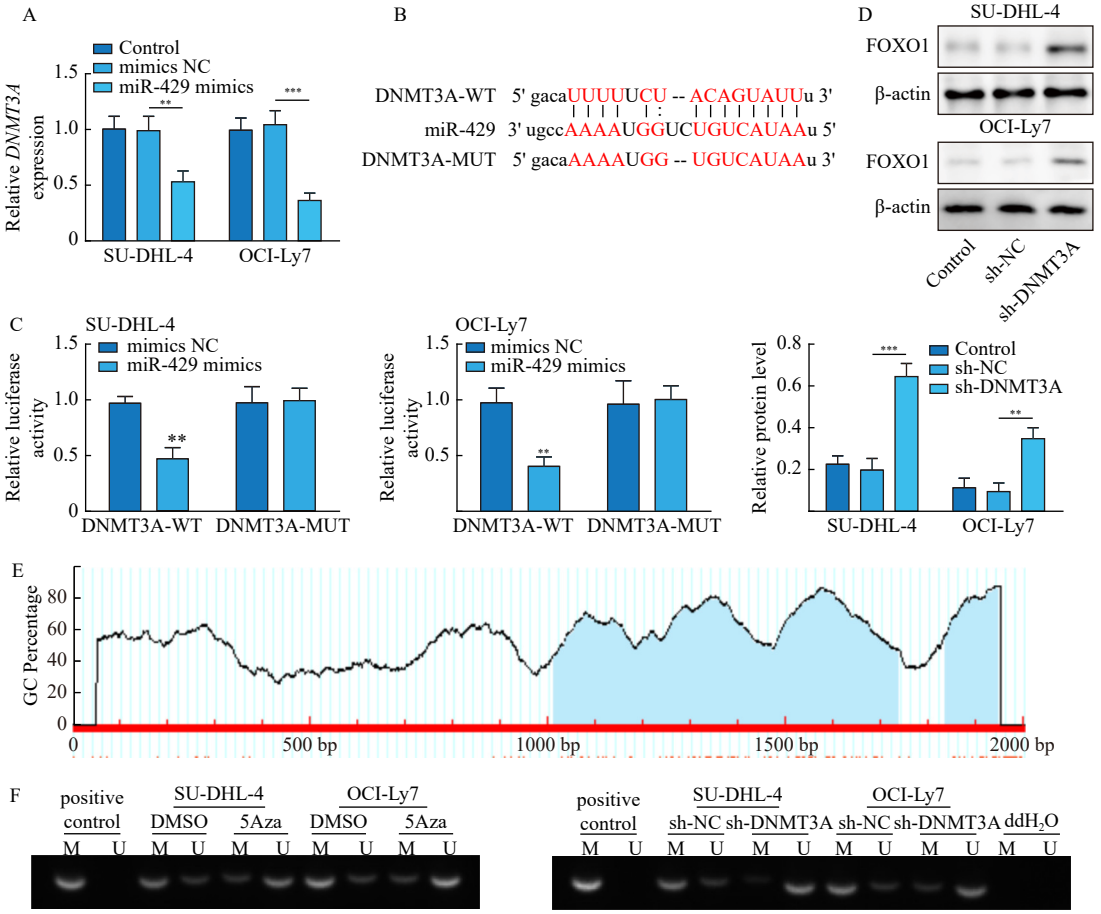

Fig. 5 miR-429 regulated FOXO1 expression by directly binding to DNMT3A. A. DLBCL cell lines SU-DHL-4 and OCI-Ly7 were transfected with either mimic-NC or miR-429 mimics. The expressions of DNMT3A were detected by RT-qPCR. B. Schematic image showed the potential binding site between miR-429 and DNMT3A. C. The luciferase reporter assay was used to measure the luciferase activity in DLBCL cell lines SU-DHL-4 and OCI-Ly7. D. Western blotting assays measured the protein levels of FOXO1 in DLBCL cell lines SU-DHL-4 and OCI-Ly7. E. The bioinformatics analysis showed that the promoter of FOXO1 contained a CpG island. F. The methylation of the FOXO1 promoter was determined by methylation-specific PCR (MSP). Data are representative of three independent experiments. $^{**}P < 0.01$, $^{***}P < 0.001$ *vs* the corresponding control.

fied CGIs at positions 122–261 and 878–1133. Methylation-specific PCR (MSP) demonstrated that both 5Aza treatment and DNMT3A knockdown *via* sh-DNMT3A transfection significantly reduced miR-429 methylation. These findings suggest a regulatory feedback loop where DNMT3A influences the expression of miR-429, which in turn modulates DNMT3A expression, impacting the autophagic and epigenetic regulation in DLBCL.

PA influenced the progression of DLBCL via miR-429, directly targeting DNMT3A to regulate autophagy.

In our study, we investigated the effects of palmitic acid (PA) treatment on the expression of miR-429, DNMT3A, and FOXO1 in SU-DHL-4 and OCI-Ly7 cells following transfections with various inhibitors and shRNAs. We used NC inhibitor, miR-429 inhibitor, sh-NC, sh-DNMT3A, and a combination of miR-429 inhibitor + sh-DNMT3A. Results indicated that PA treatment significantly upregulated miR-429 and FOXO1 while downregulating DNMT3A expression, as shown in Figs. 6A–6C. The miR-429 inhibitor decreased the levels of miR-429 and FOXO1 but increased DNMT3A levels. DNMT3A knockdown specifically reduced DNMT3A expression and increased FOXO1 levels but did not affect miR-429 levels. Notably, inhibition of miR-429 mitigated the PA-induced increase in miR-429 levels and restored the DNMT3A levels reduced by sh-DNMT3A transfection. MTS assay showed that inhibiting miR-429 could reverse the PA-induced increase in cell death. Conversely, suppression of DNMT3A expression significantly reduced cell viability and enhanced cell mortality, as confirmed by flow cytometry (Figs. 6D–6E). Transfections with inhibitor NC, miR-429 inhibitor, sh-NC, sh-DNMT3A, and the combination of miR-429 inhibitor + sh-DNMT3A demonstrated that PA-induced autophagic flux was significantly reversed by the miR-429 inhibitor, which effectively counteracted the PA-induced increase in autophagic activity. Knockdown of DNMT3A by sh-DNMT3A further enhanced the PA-induced autophagic flux, an effect that was reversed by the miR-429 inhibitor in both SU-DHL-4 and OCI-Ly7 cells (Fig. 6F). Furthermore, PA treatment markedly increased LC3 conversion (LC3-I to LC3-II), while decreasing phosphorylation of mTOR at ser2448

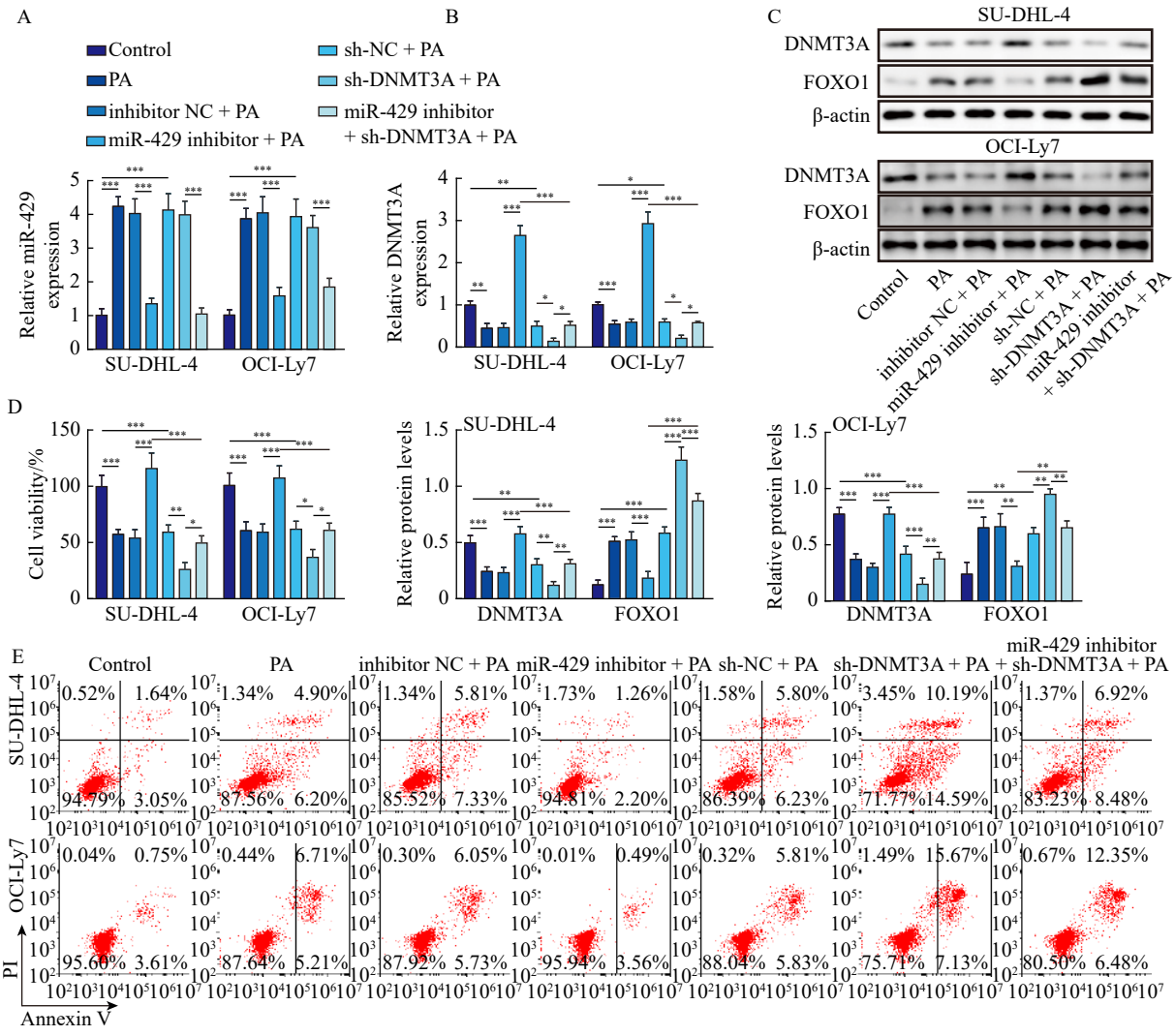

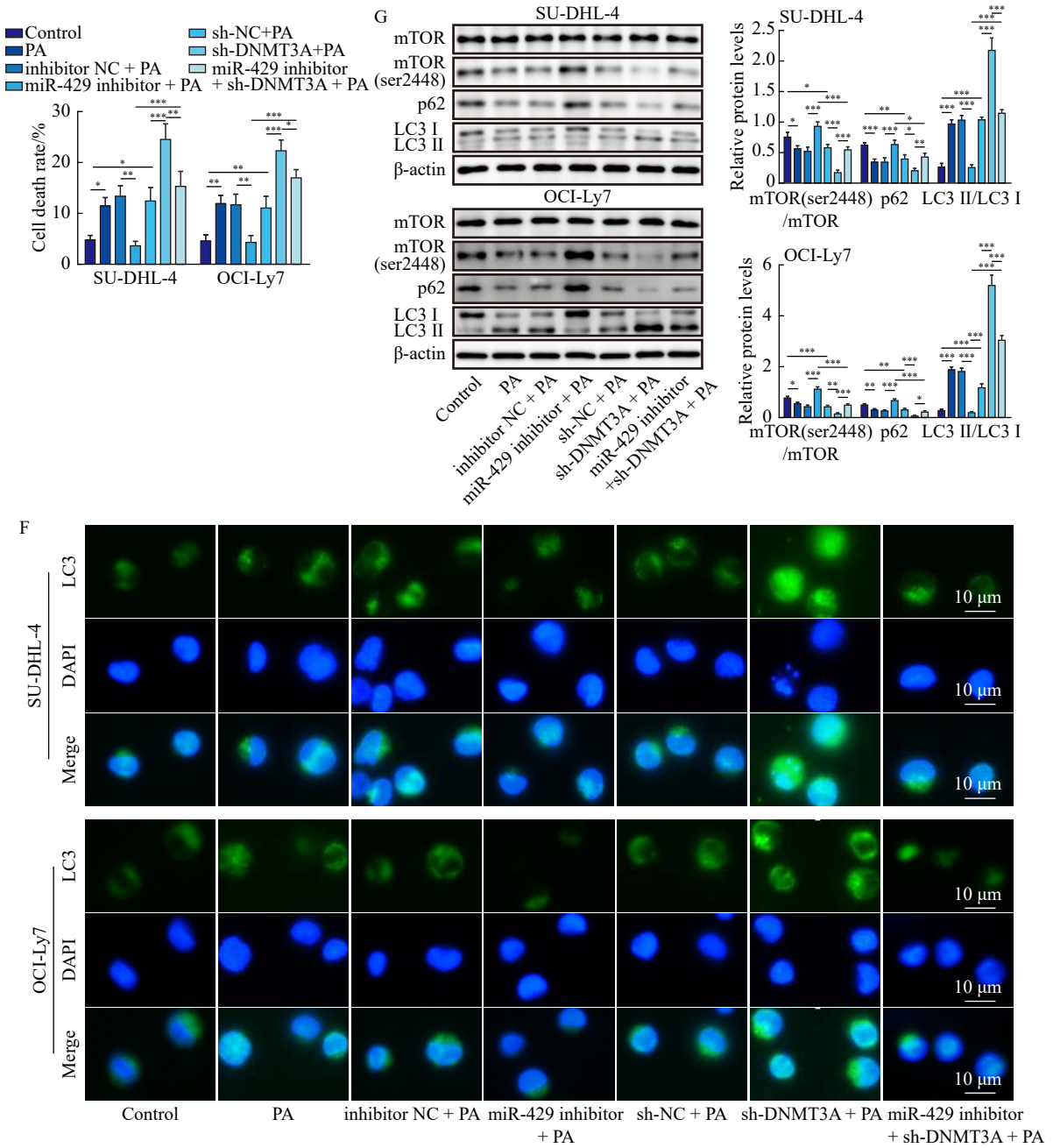

Fig. 6 PA influenced the progression of DLBCL *via* miR-429, directly targeting DNMT3A to regulate autophagy. DLBCL cell lines SU-DHL-4 and OCI-Ly7 were transfected with NC-inhibitor, miR-429 inhibitor, sh-NC, sh-DNMT3A, or miR-429 inhibitor + sh-DNMT3A, followed by the treatment of PA or vehicle for further 24 h. A–B. The expressions of miR-429 and DNMT3A were measured by RT-qPCR. C. Western blotting assay detected the protein levels of DNMT3A and FOXO1. D. The cell viability was assessed by MTS assay. E. The cell mortality was analyzed by flow cytometry assay. F. The autophagic flux was detected by immunofluorescent staining using the autophagy-specific antibody LC3 in both SU-DHL-4 and OCI-Ly7 cells after the treatment with control, PA, inhibitor-NC + PA, miR-429 inhibitor + PA, sh-NC + PA, sh-DNMT3A + PA or miR-429 inhibitor + sh-DNMT3A + PA. Scale bar = 10 μm. G. The protein levels of mTOR, mTOR(ser2448), p62, and LC3II/I were detected by Western blotting assay. Data are representative of three independent experiments. $^{*}P < 0.05$, $^{**}P < 0.01$, $^{***}P < 0.001$ *vs* the corresponding control.

and reducing p62 levels (Fig. 6G). However, the miR-429 inhibitor upregulated mTOR ser2448 phosphorylation, increased p62 levels, and decreased LC3 conversion, inhibiting autophagosome formation (Fig. 6G). Interestingly, DNMT3A knockdown attenuated autophagy. When cells were co-transfected with the miR-429 inhibitor and sh-DNMT3A, autophagy was considerably enhanced compared to cells with only miR-429 inhibition (Fig. 6G), suggesting that PA activates the miR-429/DNMT3A/FOXO1 axis to promote autophagy. These findings elucidate the dynamic regulatory roles

of miR-429, DNMT3A, and FOXO1 in modulating autophagy in response to PA treatment, highlighting potential therapeutic targets for modulating autophagy in DLBCL.

PA suppressed the development of DLBCL in vivo by regulating the miR-429/DNMT3A/FOXO1 axis.

To further investigate whether palmitic acid (PA) regulates the miR-429/DNMT3A/FOXO1 axis to promote autophagy and suppress diffuse large B-cell lymphoma (DLBCL) progression, we developed mouse tumor-bearing models. BALB/c mice were subcutaneously injected with 1×10^7 OCI-Ly7 cells suspended in 100 μL sterile 1 × PBS. The mice were then treated with either 200 mg·kg^{-1} of PA or vehicle control *via* intraperitoneal injection three times per week for two consecutive weeks. As illustrated in Figs. 7A–7B, although tumor weights increased within 25 days post-cell injection in both groups, PA treatment significantly reduced tumor growth from day 10 compared to the control group. Upon euthanasia, tumor weights were measured, revealing a

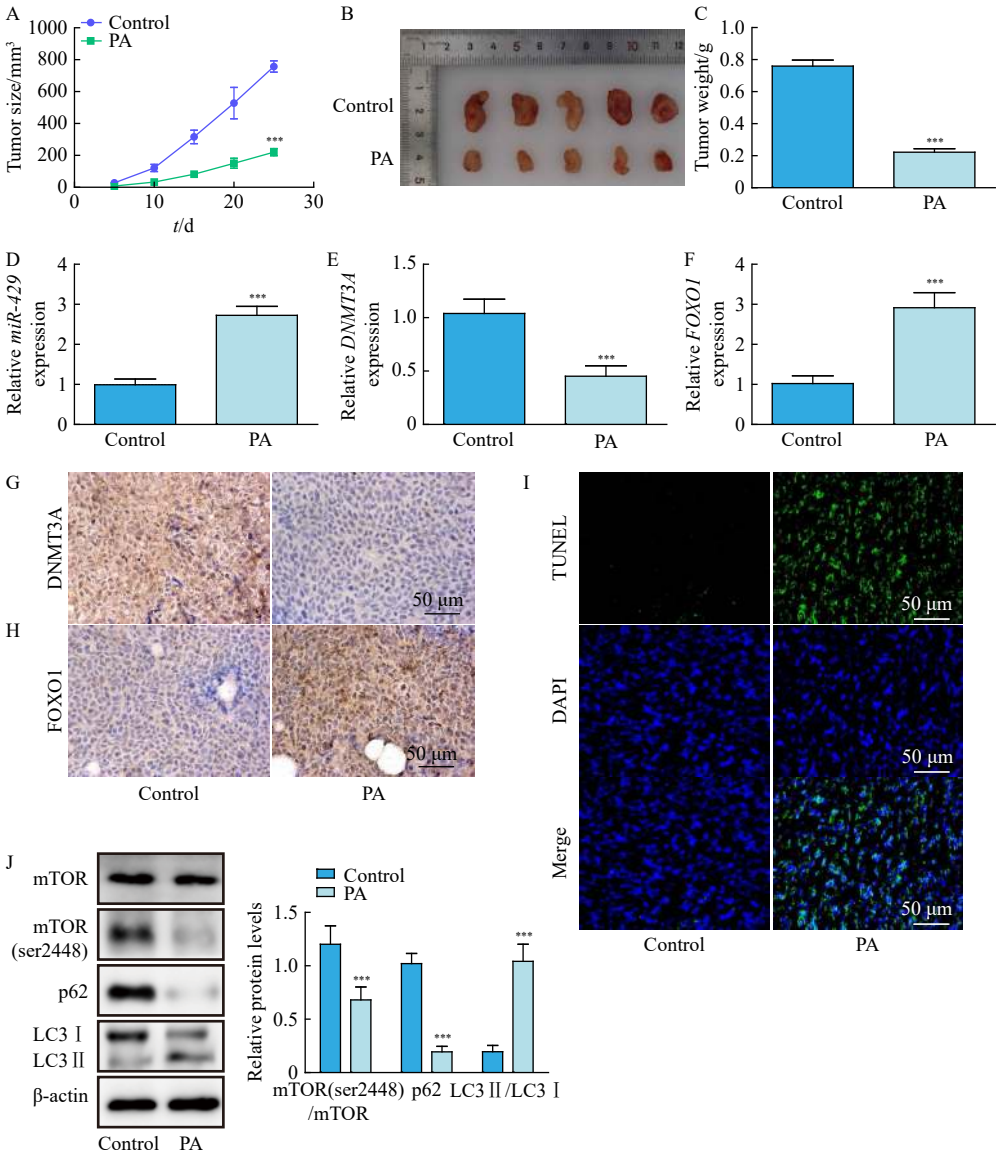

Fig. 7 PA suppressed the development of DLBCL *in vivo* by regulating the miR-429/DNMT3A/FOXO1 axis. BALB/c mice (4 weeks old) were subcutaneously injected with 100 μL OCI-Ly7 cells (1×10^7) into the right rear flank of each mouse. For the control group, an equal amount of saline solution (100 μL) was injected into the right rear flank of each mouse. After cell injections, the mice were intraperitoneally injected with sterile saline or PA (200 mg·kg^{-1}), three times per week for two weeks. After saline or PA administration, mice were observed for tumor volumes until day 25. After sacrifice, tumors were weighed and collected for further analysis. （A–C）The tumor size, volume, and weight were measured. （D–F） The expressions of *miR-429*, *DNMT3A*, and *FOXO1* were measured by RT-qPCR. （G–H）The expressions of DNMT3A and FOXO1 were analyzed by immunohistochemistry. Scale bar = 50 μm. I. The dead cells were analyzed by TUNEL staining. Scale bar = 50 μm. J. The protein levels of mTOR, mTOR(ser2448), p62, and LC3II/I were detected by Western blotting assay. Data are representative of three independent experiments. $^{***}P < 0.001$ *vs* the corresponding control.

significant decrease in tumor mass in the PA-treated group (Fig. 7C). Further analyses were conducted on the excised tumor tissues. RT-qPCR results indicated that PA treatment markedly upregulated miR-429 and FOXO1 levels while downregulating DNMT3A expression (Figs. 7D–7F). Immunohistochemical analysis further supported these findings, showing decreased DNMT3A and increased FOXO1 expression in the PA-treated tumors (Figs. 7G–7H), which underscores the involvement of the PA-regulated DNMT3A/FOXO1 pathway in DLBCL development. Cell mortality within the tumors was assessed using a TUNEL assay, which demonstrated a significant increase in cell death in the PA-treated group compared to controls (Fig. 7I). Additionally, Western blotting analysis revealed that PA treatment significantly reduced the levels of phosphorylated mTOR (ser2448) and p62, while increasing the ratio of LC3II to LC3I (Fig.7J). These findings suggest that PA enhances autophagy, evidenced by changes in autophagy-related protein expression. Taken together, these results confirm that PA promotes cell autophagy and suppresses tumor growth by modulating the miR-429/DNMT3A/FOXO1 axis in DLBCL. This indicates a promising therapeutic potential for PA in the treatment of DLBCL, leveraging the autophagic pathway.

Discussion

DLBCL is the most common type of non-Hodgkin lymphoma (NHL), accounting for approximately one-third of all NHL cases globally [1]. While around 60% of DLBCL patients respond positively to R-CHOP (rituximab, cyclophosphamide, doxorubicin, vincristine, and prednisone) immunochemotherapy, overall survival rates remain suboptimal [24-28]. The heterogeneity and complex pathogenesis of DLBCL often result in treatment resistance, leading to poor clinical outcomes [4, 29]. Thus, there is a critical need for novel therapeutic agents to improve treatment options for DLBCL patients. In this study, we investigated the effects of PA, a prominent type of free fatty acids (FFAs), on the progression of DLBCL. Our results showed that in DLBCL tissues, the levels of miR-429 and FOXO1 were downregulated, while DNMT3A was upregulated compared to normal control tissues. Treatment with PA upregulated miR-429 and FOXO1, downregulated DNMT3A in DLBCL cell lines, and stimulated autophagic activity by increasing the expression of autophagy-related proteins. Further *in vitro* and *in vivo* experiments demonstrated that PA-induced autophagy was mediated through direct regulation of the miR-429/DNMT3A/FOXO1 axis. Our findings initially indicate that targeting the miR-429/DNMT3A/FOXO1 axis may represent a viable therapeutic strategy to treat DLBCL, offering the potential for enhanced patient outcomes.

PA is a prevalent fatty acid in the human diet, known to participate in various biological pathways relevant to cancer progression. It has been implicated in histone methylation, which can potentiate metastasis initiation [30], in regulating β-oxidation processes that influence tumor growth [31], and in stabilizing oncogenic proteins to promote tumor progression [32]. MiR-429, a member of the miR-200 family, is involved in numerous biological processes, including cell apoptosis, proliferation, invasion, metastasis, and drug resistance in several cancers, including DLBCL [15]. Previous studies have shown that PA could induce the expression of miR-429 [33]. In this study, our findings indicated that miR-429 was significantly downregulated in DLBCL tissues. Treatment with PA led to increased levels of miR-429 and enhanced cell death, suggesting that miR-429 may play a critical role in PA-induced cell mortality.

MicroRNAs are crucial post-transcriptional regulators implicated in various stages of cancer development [34], influencing gene translation efficiency and mRNA stability [35, 36]. In this study, bioinformatics analysis using StarBase 2.0 (https://starbase.sysu.edu.cn/) predicted a potential binding site for miR-429 within the DNMT3A gene sequence. We conducted luciferase reporter assays and methylation-specific PCR in DLBCL cell lines transfected with either WT-DNMT3A or MUT-DNMT3A, alongside miR-429 mimics or mimic-NC. These experiments validated that miR-429 directly targets DNMT3A, leading to its downregulation in DLBCL. Previous chromatin immunoprecipitation assays have shown that DNMT3A directly binds within the FOXO1 region, indicating a regulatory interaction [37]. Further experiments confirmed that silencing DNMT3A upregulates FOXO1, a key regulator of autophagy [38]. To explore whether PA promotes cell death or autophagy *via* the miR-429/DNMT3A/FOXO1 axis, we co-transfected cells with miR-429 inhibitor and sh-DNMT3A, followed by PA treatment. Results demonstrated that inhibiting miR-429 increased DNMT3A and decreased FOXO1 levels compared to the control. However, the knockdown of DNMT3A reversed the effects of the miR-429 inhibitor, underscoring that elevated levels of miR-429 induced by PA contribute to cell autophagy by downregulating DNMT3A and upregulating FOXO1. Our findings suggest that the PA-activated miR-429/DNMT3A/FOXO1 axis offers a novel therapeutic target for DLBCL. To further validate PA's regulatory effects on tumorigenesis *in vivo*, we established tumor-bearing mouse models and administered PA significantly suppressed tumor growth by enhancing autophagy, mediated through the activation of the miR-429/DNMT3A/FOXO1 pathway. This evidence points to a promising approach for DLBCL treatment, leveraging dietary components to influence molecular pathways critical for tumor suppression.

In conclusion, our research demonstrated that DLBCL is characterized by low levels of miR-429 and FOXO1 and elevated levels of DNMT3A. Treatment with PA increases miR-429 and FOXO1 while decreasing DNMT3A in DLBCL cell lines. Mechanistically, PA facilitates cell autophagy by directly upregulating miR-429, which inactivates the DNMT3A/FOXO1 axis both *in vitro* and *in vivo*, leading to the suppression of DLBCL progression. Our findings provide initial evidence that PA mitigates DLBCL progression by

modulating the miR-429/DNMT3A/FOXO1 axis, presenting a novel avenue for therapeutic intervention in DLBCL. Future investigations should focus on validating the role of the PA-induced activation of the miR-429/DNMT3A/FOXO1 axis in additional clinical specimens to further substantiate this potential treatment strategy.

References

[1] Sehn LH, Salles G. Diffuse large B-Cell lymphoma [J]. *N Engl J Med*, 2021, **384**(9): 842-858.

[2] Cheson BD, Nowakowski G, Salles G. Diffuse large B-cell lymphoma: new targets and novel therapies [J]. *Blood Cancer J*, 2021, **11**(4): 68.

[3] Schmitz R, Wright GW, Huang DW, *et al*. Genetics and pathogenesis of diffuse Large B-Cell Lymphoma [J]. *N Engl J Med*, 2018, **378**(15): 1396-1407.

[4] He MY, Kridel R. Treatment resistance in diffuse large B-cell lymphoma [J]. *Leukemia*, 2021, **35**(8): 2151-2165.

[5] Urso CJ, Zhou H. Palmitic acid lipotoxicity in microglia cells is ameliorated by unsaturated fatty acids [J]. *Int J Mol Sci*, 2021, **22**(16): 9093.

[6] Zhu S, Jiao W, Xu Y, *et al*. Palmitic acid inhibits prostate cancer cell proliferation and metastasis by suppressing the PI3K/Akt pathway [J]. *Life Sci*, 2021, **286**: 120046.

[7] Binker-Cosen MJ, Richards D, Oliver B, *et al*. Palmitic acid increases invasiveness of pancreatic cancer cells AsPC-1 through TLR4/ROS/NF-κB/MMP-9 signaling pathway [J]. *Biochem Biophys Res Commun*, 2017, **484**(1): 152-158.

[8] Maly IV, Hofmann WA. Effect of palmitic acid on exosome-mediated secretion and invasive motility in prostate cancer cells [J]. *Molecules*, 2020, **25**(12): 2722.

[9] Tu QQ, Zheng RY, Li J, *et al*. Palmitic acid induces autophagy in hepatocytes *via* JNK2 activation [J]. *Acta Pharmacol Sin*, 2014, **35**(4): 504-512.

[10] Yu DY, Zhao QL, Furuta M, *et al*. Molecular mechanisms of apoptosis induction by 2-dodecylcyclobutanone, a radiolytic product of palmitic acid, in human lymphoma U937 cells [J]. *Apoptosis*, 2012, **17**(6): 636-645.

[11] Roy SG. Regulation of autophagy by miRNAs in human diseases [J]. *Nucleus (Calcutta)*, 2021, **64**(3): 317-329.

[12] Feng Y, Zhong M, Zeng S, *et al*. Exosome-derived miRNAs as predictive biomarkers for diffuse large B-cell lymphoma chemotherapy resistance [J]. *Epigenomics*, 2019, **11**(1): 35-51.

[13] Zhang L, Liu Q, Mu Q, *et al*. MiR-429 suppresses proliferation and invasion of breast cancer *via* inhibiting the Wnt/β-catenin signaling pathway [J]. *Thorac Cancer*, 2020, **11**(11): 3126-3138.

[14] Liu D, Song L, Dai Z, *et al*. MiR-429 suppresses neurotrophin-3 to alleviate perineural invasion of pancreatic cancer [J]. *Biochem Biophys Res Commun*, 2018, **505**(4): 1077-1083.

[15] Liang Y, Yu ZJ, Liu M, *et al*. hsa-miR-429 targets CBX8 to promote cell apoptosis in diffuse large B-cell lymphoma [J]. *Mol Med Rep*, 2021, **24**(6).

[16] Getaneh Z, Asrie F, Melku M. MicroRNA profiles in B-cell non-Hodgkin lymphoma [J]. *Ejifcc*, 2019, **30**(2): 195-214.

[17] Li E, Zhang Y. DNA methylation in mammals [J]. *Cold Spring Harb Perspect Biol*, 2014, **6**(5): a019133.

[18] Chambwe N, Kormaksson M, Geng H, *et al*. Variability in DNA methylation defines novel epigenetic subgroups of DLBCL associated with different clinical outcomes [J]. *Blood*, 2014, **123**(11): 1699-1708.

[19] Bakhshi TJ, Georgel PT. Genetic and epigenetic determinants of diffuse large B-cell lymphoma [J]. *Blood Cancer J*, 2020, **10**(12): 123.

[20] Dhanak D, Jackson P. Development and classes of epigenetic drugs for cancer [J]. *Biochem Biophys Res Commun*, 2014, **455**(1-2): 58-69.

[21] Zhao H, Zhang LE, Guo S, *et al*. Overexpression of DNA methyltransferase 1 as a negative independent prognostic factor in primary gastrointestinal diffuse large B-cell lymphoma treated with CHOP-like regimen and rituximab [J]. *Oncol Lett*, 2015, **9**(5): 2307-2312.

[22] Mancini M, Grasso M, Muccillo L, *et al*. DNMT3A epigenetically regulates key microRNAs involved in epithelial-to-mesenchymal transition in prostate cancer [J]. *Carcinogenesis*, 2021, **42**(12): 1449-1460.

[23] Hegde M, Joshi MB. Comprehensive analysis of regulation of DNA methyltransferase isoforms in human breast tumors [J]. *J Cancer Res Clin Oncol*, 2021, **147**(4): 937-971.

[24] Li S, Young KH, Medeiros LJ. Diffuse large B-cell lymphoma [J]. *Pathology*, 2018, **50**(1): 74-87.

[25] Duan Q, Li Y, Ou L, *et al*. Global research trends on the treatment of diffuse large B-Cell lymphoma: a bibliometric and visualized study [J]. *J Cancer*, 2022, **13**(6): 1785-1795.

[26] Song Y, Zhou H, Zhang H, *et al*. Efficacy and safety of the biosimilar IBI301 plus standard CHOP (I-CHOP) in comparison with Rituximab plus CHOP (R-CHOP) in patients with previously untreated diffuse large B-Cell lymphoma (DLBCL): a randomized, double-blind, parallel-group, phase 3 trial [J]. *Adv Ther*, 2021, **38**(4): 1889-1903.

[27] Hu J, Xu J, Yu M, *et al*. An integrated prognosis model of pharmacogenomic gene signature and clinical information for diffuse large B-cell lymphoma patients following CHOP-like chemotherapy [J]. *J Transl Med*, 2020, **18**(1): 144.

[28] Li X, Huang H, Xu B, *et al*. Dose-dense Rituximab-CHOP versus Standard Rituximab-CHOP in newly diagnosed Chinese patients with diffuse large B-Cell lymphoma: a randomized, multicenter, open-label phase 3 trial [J]. *Cancer Res Treat*, 2019, **51**(3): 919-932.

[29] Liu Y, Zeng L, Zhang S, *et al*. Identification of differentially expressed proteins in chemotherapy-sensitive and chemotherapy-resistant diffuse large B cell lymphoma by proteomic methods [J]. *Med Oncol*, 2013, **30**(2): 528.

[30] Alkan HF, Altea-Manzano P, Fendt SM. Palmitic acid: enabling the tumor's nerves [J]. *Cell Metab*, 2022, **34**(1): 7-9.

[31] Beloribi-Djefaflia S, Vasseur S, Guillaumond F. Lipid metabolic reprogramming in cancer cells [J]. *Oncogenesis*, 2016, **5**(1): e189.

[32] Fiorentino M, Zadra G, Palescandolo E, *et al*. Overexpression of fatty acid synthase is associated with palmitoylation of Wnt1 and cytoplasmic stabilization of beta-catenin in prostate cancer [J]. *Lab Invest*, 2008, **88**(12): 1340-1348.

[33] Nguyen MT, Min KH, Lee W. Palmitic acid-induced miR-429-3p impairs myoblast differentiation by downregulating CFL2 [J]. *Int J Mol Sci*, 2021, **22**(20): 10972.

[34] Thorsen SB, Obad S, Jensen NF, *et al*. The therapeutic potential of microRNAs in cancer [J]. *Cancer J*, 2012, **18**(3): 275-284.

[35] Afonso-Grunz F, Müller S. Principles of miRNA-mRNA interactions: beyond sequence complementarity [J]. *Cell Mol Life Sci*, 2015, **72**(16): 3127-3141.

[36] Cottrell KA, Szczesny P, Djuranovic S. Translation efficiency is a determinant of the magnitude of miRNA-mediated repression [J]. *Sci Rep*, 2017, **7**(1): 14884.

[37] Jiang Y, Zhu H, Chen Z, *et al*. Hepatic IGF2/H19 epigenetic alteration induced glucose intolerance in gestational diabetes mellitus offspring *via* FoxO1 mediation [J]. *Front Endocrinol (Lausanne)*, 2022, **13**: 844707.

[38] Zhao Y, Yang J, Liao W, *et al*. Cytosolic FoxO1 is essential for the induction of autophagy and tumour suppressor activity [J]. *Nat Cell Biol*, 2010, **12**(7): 665-675.

Cite this article as: LI Weiming, GAO Ming, XUE Weili, *et al*. Palmitic acid reduces the methylation of the FOXO1 promoter to suppress the development of diffuse large B-cell lymphoma *via* modulating the miR-429/DNMT3A axis [J]. *Chin J Nat Med*, 2024, **22**(6): 554-567.